Available online at www.sciencedirect.com

ScienceDirect

Procedia Materials Science 3 (2014) 135 – 140

Procedia Materials Science

www.elsevier.com/locate/procedia

20th European Conference on Fracture (ECF20)

Simulation of cyclic plastic behavior of 304L steel using the crystal plasticity finite element method

Jiawa Lu[a*], Adib Becker[a], Wei Sun[a], David Tanner[b]

[a] *Faculty of Engineering, The University of Nottingham, University Park, Nottingham, NG7 2RD, UK*
[b] *University of Bristol, Clifton, BS8 1TR, UK*

Abstract

The stabilised cyclic plasticity behaviour of 304L austenitic stainless steel at room temperature is studied by using the multiscale crystal plasticity finite element method within the software ABAQUS. The physical-based material constitutive equations are coded in the UMAT user-subroutine. A polycrystal model is constructed and is shown to be able to approximate the macroscale cyclic plasticity behaviour. The distributions of stress, strain and plastic dissipation energy are examined locally to investigate their relationship with the possible crack initiation sites, and the effects of grain orientation. The effects of grain boundaries are also studied by studying the distribution of dislocation density and the number of active slip systems.

Selection and peer-review under responsibility of the Norwegian University of Science and Technology (NTNU), Department of Structural Engineering

Keywords: Crystal plasticity; Finite Element; Cyclic plasticity; 304L steel;

Nomenclature

$\boldsymbol{L}$	Velocity gradient	V	Volume	γ	Shear strain
$\boldsymbol{F}$	Deformation gradient	G	Shear Modulus	τ	Shear stress
$\boldsymbol{\sigma}$	Stress	b	Burger's vector	τ_c	Critical shear stress
$\boldsymbol{\varepsilon}$	Strain	Δ	Range	χ	Backstress
$\boldsymbol{m}$	Slip direction	*	Lattice deformation	ρ	Dislocation density
$\boldsymbol{n}$	Slip normal	p	Plastic deformation	α, β	Index of slip system
C_{ij}	Elastic Moduli	$\boldsymbol{A}$	Dislocation interaction matrix, indexed by a_1 to a_5.		

* Corresponding author. *E-mail address:* eaxjl2@nottingham.ac.uk

Selection and peer-review under responsibility of the Norwegian University of Science and Technology (NTNU), Department of Structural Engineering
doi:10.1016/j.mspro.2014.06.025

1. Introduction

304L steel is a type of austenitic stainless steel widely used in pipes of chemical plants, which may be subject to cyclic loading conditions. The predictions of fatigue life and crack initiation sites are important aspects of designing the plant structure.

A uniaxial fatigue test from literature (Le Pécheur et al., 2012b) was conducted at the room temperature under a strain rate of $4 \times 10^{-3} s^{-1}$ for a strain range of $\pm 0.2\%$. Macroscopically, the Chaboche elasto-plasticity model is able to predict the elasto-plastic material behaviour, when the stress amplitude in a fatigue test is influenced by dislocation multiplication and annihilation only. However, in the final stage of fatigue life, the material behaviour largely depends on the microstructure. It has been pointed out by several authors (Dunne et al., 2007, Bieler et al., 2009, Lin et al., 2011) that microcracks initiate at the grain boundaries and slip traces, and propagate along the slip direction. In order to simulate the influence of microscopic factors on the macroscale material behaviour, the crystal plasticity finite element method (CPFEM) is used here (Roters et al., 2010). The microscopic factors usually involve slip with the associated dislocation, texture and grain shapes. Therefore, two main stages are required in the crystal plasticity framework: the first is the constitutive description of the single crystal mechanical response, and the second is a transition from the microscopic to the macroscopic behaviour.

The microcrack initiation and fatigue life prediction methods are usually based on stress, strain or hysteresis plastic energy (Anahid et al., 2011). All these variables are obtained from the steady state cyclic behaviour, instead of the transient cyclic hardening or softening (Ellyin, 1997). These variables are presented in this paper to examine their local distribution based on CPFEM, and to investigate their relationship with the possible microcrack initiation sites.

2. Theory

2.1. Single crystal constitutive equations

The deformation gradient $\boldsymbol{F}$ can be decomposed into a lattice deformation gradient $\boldsymbol{F}^*$ and a plastic deformation gradient $\boldsymbol{F_p}$, by assuming that the material flows due to dislocation motion, and then the combination of elastic deformation and rigid body rotation (Roters et al., 2010):

$$\boldsymbol{F} = \boldsymbol{F}^* \boldsymbol{F_p} \tag{1}$$

The velocity gradient $\boldsymbol{L}$ is defined as

$$\boldsymbol{L} = \dot{\boldsymbol{F}} \boldsymbol{F}^{-1} = \dot{\boldsymbol{F}}^* \boldsymbol{F}^{*-1} + \boldsymbol{F}^* \dot{\boldsymbol{F}}_{\boldsymbol{p}} \boldsymbol{F}_{\boldsymbol{p}}^{-1} \boldsymbol{F}^{*-1} = \boldsymbol{L}^* + \boldsymbol{F}^* \boldsymbol{L_p} \boldsymbol{F}^{*-1} \tag{2}$$

The plastic velocity tensor $\boldsymbol{L_p}$ is expressed by the sum of the shearing rate $\dot{\gamma}^\alpha$ for all the available 12 slip systems of a face centred cubic (FCC) crystal structure ($\alpha = 1,2, \dots 12$). The slip system α is specified by the slip direction $\boldsymbol{m}^\alpha$ and slip plane normal $\boldsymbol{n}^\alpha$ in the global coordinate, as follows:

$$\boldsymbol{L_p} = \sum_{\alpha=1}^{12} \dot{\gamma}^\alpha \, \boldsymbol{m}^\alpha \otimes \boldsymbol{n}^\alpha \tag{3}$$

The shearing rate $\dot{\gamma}^\alpha$ for the slip system α can be approximated by a power law, as follows:

$$\dot{\gamma}^\alpha = \dot{\gamma}_0 \left(\frac{|\tau^\alpha - \chi^\alpha|}{\tau_c^\alpha} \right)^n sign(\tau^\alpha - \chi^\alpha) \tag{4}$$

where the rate exponent n controls the strain rate sensitivity. The critical resolved shear stress τ^α for the slip system α is the projection of the nominal stress onto the slip plane, and it is the driving force of the plastic deformation. The backstress χ^α satisfies the nonlinear evolution rule:

$$\dot{\chi}^\alpha = C\dot{\gamma} - D\chi^\alpha |\dot{\gamma}^\alpha| \tag{5}$$

The strength τ_c^α for the slip system α represents the resistance of the plastic deformation, or the stress necessary to attain reference velocity for the slip system α. In the physical based hardening law (Harder, 1999), it is assumed that the dislocation cutting force is the major obstacle in plastic deformation, and the plastic shear rate is related to the mean effect of the mobile dislocation density. The critical shear stress τ_c^α is thus formulated with regards to the forest dislocation ρ_F, such that:

$$\tau_c^\alpha = Gb \sqrt{\sum_{\beta=1}^{12} A^{\alpha\beta} \rho_F^\beta} = \sum_\beta h_{\alpha\beta} |\gamma^\beta| \tag{6}$$

where $\boldsymbol{A}$ is the interaction matrix, which describes the extent of hindering between different types of slip systems.

The entries of the interaction matrix are indexed by five dislocation interaction types proposed by Bassani and Wu (1991), from a_1 to a_5. The dislocation density evolution law is able to describe the dislocation multiplication and annihilation for the slip system α, as follows:

$$\dot{\rho}_F^{\alpha} = \frac{|\dot{\gamma}^{\alpha}|}{b}\left[\frac{\sqrt{\sum_{\alpha\neq\beta}\rho_F^{\beta}}}{K} - 2y_c\rho^{\alpha}\right] \quad (7)$$

where b is the Burgers vector. The first term controls the dislocation formation, and the constant y_c represents the critical annihilation length, which is related to dynamic recovery.

2.2. Polycrystal morphology and homogenization method

CPFEM uses continuum mechanics theory by incorporating a statistical model in the simulating process. A representative volume element (RVE) with a few grains is chosen here to represent the macroscopic polycrystalline aggregate containing the order of billions of grains. The minimum grain size of the RVE depends on the loading conditions and the material texture.

A homogenization method should be used to transit the output from the micro-scale to the macro-scale. For example, the macroscale stress $\overline{\boldsymbol{\sigma}}$ and strain $\overline{\boldsymbol{\varepsilon}}$ are the volume-averaged values computed from the local stress and strain of the whole domain $\mathcal{B}$ as follows:

$$\overline{\boldsymbol{\sigma}} = \frac{1}{V}\int_{\mathcal{B}} \boldsymbol{\sigma}\, dV \quad and \quad \overline{\boldsymbol{\varepsilon}} = \frac{1}{V}\int_{\mathcal{B}} \boldsymbol{\varepsilon}\, dV \quad (8)$$

3. **Results**

A 3D cuboid shape (Figure 1*a*) with dimensions of $200\mu m \times 200\mu m \times 50\mu m$ including 25 grains is created in this study, whose grain shape was constructed by the Voronoi tessellation algorithm available in the MATLAB software. The average grain size is $50\mu m$. It is subjected to a loading within the strain range $\pm 0.2\%$ in the y-direction on Face 1. Face 2 is fixed in the x, y and z directions to prevent rigid body motion. The element type used is a 3D hexagonal linear continuum element (C3D8 in ABAQUS).

304L steel has a FCC crystal structure. The material constants are extracted from the literature (Le Pécheur et al., 2012a) and modified by curve fitting (Table 1). The material constitutive equations are coded in the UMAT user-subroutines within the commercially available software ABAQUS. Each grain is assigned a specific, but randomly generated orientation, which is defined by Euler angle. In total, three sets of grain orientations are used in this analysis.

Table 1. Material Constants.

C_{11}(MPa)	C_{12}(MPa)	C_{44}(MPa)	C	D	$\dot{\gamma}_0$ (s^{-1})	n	ρ_0 (mm^{-2})
261200	112000	74600	15300	430	1.00E-05	49	9.00E+06
b (mm)	y_c (mm)	K	a_1	a_2	a_3	a_4	a_5
2.54E-07	7.50E-05	1	0.625	0.045	0.045	0.137	0.122

3.1. Convergence study

The volume-averaged stress-strain loops of the second cycle in the uniaxial fatigue simulation, based on three sets of orientations, are plotted in Figure 1*b*. These results are compared to the experimental data from the literature (Le Pécheur et al., 2012a) and the macroscopic simulation based on the Chaboche model (Chaboche, 1991), which is also coded in a UMAT user-subroutine. The comparison shows that the 25-grain geometry is shown to be able to capture the key features of the macroscopic cyclic plasticity behaviour, such as isotropic and kinematic hardening, and the hysteresis loop in the first few cycles. In addition, the differences between the volume-averaged results obtained from three sets of orientations are under 5%. If the simulation involves a larger strain range, the results variation may be larger (not shown here). This is because usually 10^3 to 10^4 grains are recommended for the RVE to ensure that the grain size is large enough to predict the macroscopic properties statistically (Diard et al., 2005).

However, in this paper, the simulation is limited to the strain range of $\pm 0.2\%$, so the 25-grain geometry can be treated as the RVE.

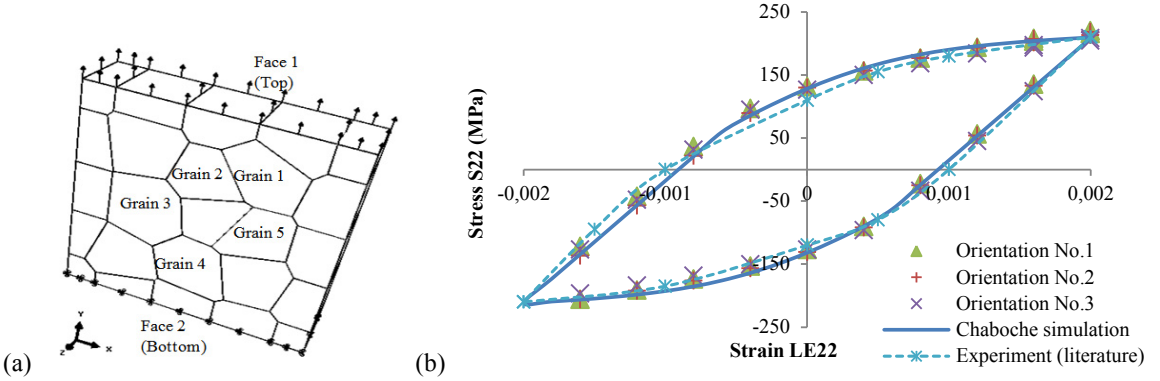

Fig.1. (a) A sketch of polycrystal model. Face 1: strain controlled y-directional loading; Face 2: fixed in the x, y, z directions; and (b) Volume-averaged stress-strain loops at the end of the second cycle from the polycrystal model based on different orientations, compared to the experimental data from literature and the macroscopic simulation based on the Chaboche model.

3.2. Local material behaviour

In analysing the local stress and strain behaviour, orientation No. 2 is chosen here. The stress-strain loops at the second loading cycle for Grains 1, 2, 3 and 4 are plotted in Figure 2*a*. By comparing the local behaviour to the volume-averaged behaviour, it shows that Grains 2 and 4, referred to as hard grains, have higher than average stress and lower than average strain. Their plastic deformation is constrained by the neighbouring soft Grains 1 and 3, which have slightly higher than average plastic deformation. The classification of hard and soft grains is determined by their orientations.

Although the loading condition of the front face (the *z* direction pointing out of the paper) and the back surface (the *z* direction pointing into the paper) are symmetric, the local stress and strain responses of these two surfaces to the cyclic loading are different (not shown here). This indicates that there is a strong intragranual heterogeneity. The distributions of stress σ_{yy} (*S22* in ABAQUS) and logarithm strain ε_{yy} (*LE22* in ABAQUS) in the y-direction for the back surfaces are plotted in Figures 2*b* and 3*a*. Soft Grains 1 and 3 exhibit strain concentration and stress relaxation, whereas their neighbouring hard Grains 2 and 4 exhibit stress concentration and lower strains. An exception is Grain 5, which exhibits both stress concentration and relaxation, although at different edges. This indicates that the highly anisotropic behaviour of a single crystal causes a grain boundary deformation to satisfy both the stress equilibrium and strain compatibility. Furthermore, the stress and strain concentration sites are determined by grain orientation and interaction.

The distribution of the plastic dissipation energy (*ELPD*) for the back surfaces is plotted in Figure 3*b*. It is shown that grains with higher values of plastic dissipation energy are mostly low in stress and high in strain in this case. However, grains with higher values of strain do not always have plastic dissipation energy concentration.

Since the plastic deformation is vital in determining the damage initiation and evolution (Dunne et al., 2007), and stress and strain concentration criteria do not tend to occur together, the strain criterion is considered to have a more direct link to the microscopic modelling of fatigue damage. As for the energy criterion, it seems to be a stricter criterion than the strain one, and they both need further experimental verification.

The distribution of the number of active slip systems is plotted in Figure 4*a*. There seems to be no obvious relationship between the number of active slip systems and the classification of soft and hard grains. However, the highest number of slip systems in this case study, 8, is only seen at the elements that lie on the grain boundary. In contrast, the interior elements of a grain tend to have a lower number of active slip systems. As an example, the distribution of the dislocation density of slip system $(111)[0\bar{1}1]$ for the back surfaces is plotted in Figure 4*b*. It is completely activated in four grains, where the projection of the nominal stress onto this slip system is highest among all other 11 slip systems. A nearly uniform dislocation density distribution can be observed in these four grains, but it is usually slightly higher at the grain boundary. There are four partially activated grains, such as Grain 5. A

negative sign can be observed for the value of the dislocation density at the relaxation position, which is not possible physically. In FE analysis, the nodal values are obtained via extrapolation and interpolation from the integration points of the element, and thus these values may not be very accurate at the grain boundary, particularly if a relatively large element is used. Both of the distributions indicate that dislocation density tends to pile up at grain boundary.

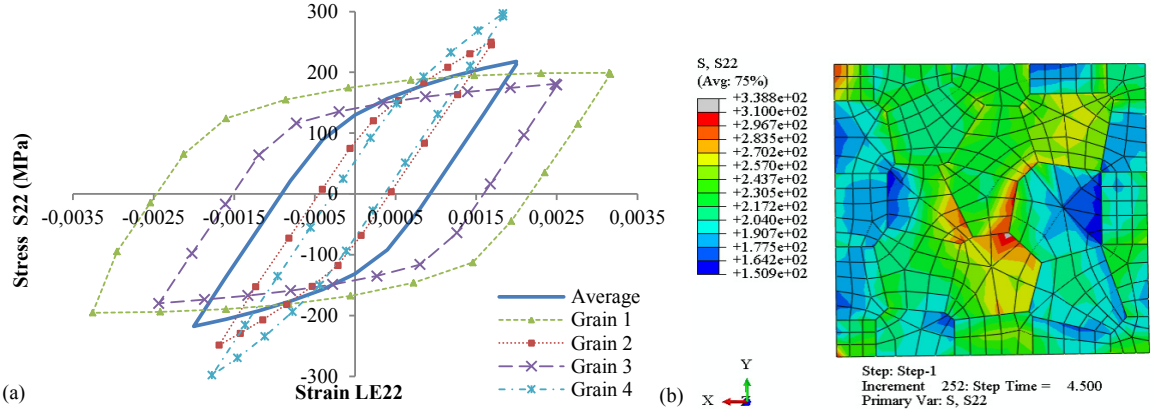

Fig.2. (a) Local and volume-averaged stress-strain curve showing the grain orientation and interaction effects; and (b) Distribution of stress in the y-direction (*S22*) on the back surface at the end of the second cycle.

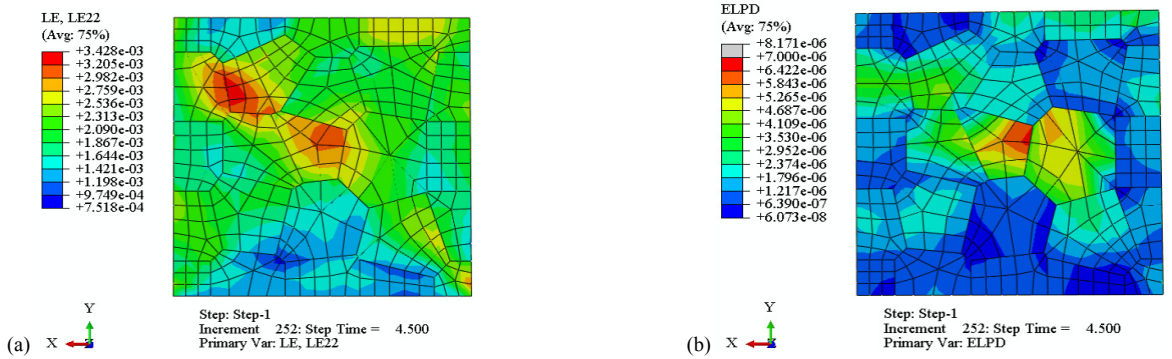

Fig.3. Field output of the back surface at the end of the second cycle: (a) Strain in the y-direction (*LE22*); and (b) Plastic dissipation energy (*ELPD*).

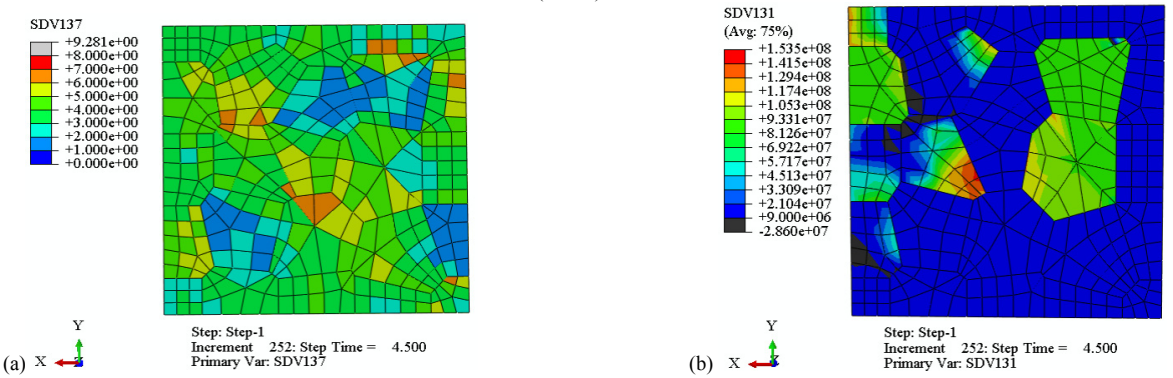

Fig.4. Field output at the end of the second cycle of the back surface: (a) Number of active slip systems (*SDV137*); and (b) Dislocation density of the slip system $(111)[0\bar{1}1]$ (*SDV131*).

4. Conclusion and future work

In order to predict the fatigue life of 304L austenitic stainless steel, the stabilised cyclic stress-strain behaviour is studied by comparing the CPFEM results to experimental data from the literature and a macroscopic simulation based on the Chaboche elasto-plasticity model. From the convergence study based on three sets of random orientations, a 25-grain layered Voronoi geometry is shown to be able to approximate the cyclic plasticity behaviour for the strain range of $\pm 0.2\%$ in the macroscale.

The local material behaviour is also examined at the end of the second cycle. Several conclusions can be summarized. Firstly, there is a large intragranular heterogeneity in all directions, and the grain local behaviour is determined by its orientation, as well as the interaction between the grains. Secondly, as observed from the results of stress and strain distributions, the grain boundary plays a vital role in satisfying stress equilibrium and strain compatibility. In addition, it is also the place where more slip systems are activated and dislocations pile up. Thirdly, stress and strain both concentrate at grain boundaries, though at neighbouring grains. Since plastic deformation is the vital reason for fatigue microcrack initiation and propagation, the strain and plastic dissipation energy criteria may be more suitable than the stress criterion.

Future work involves predicting the microcrack initiation sites based on the strain or plastic dissipation energy criterion. Meanwhile, experimental work would be needed to compare the predicted sites to the experimental results. In addition, an internal variable damage may be introduced into the constitutive equations, in order to consider the stiffness degradation during microcrack propagation. A 3D RVE with more grains may be used to enable the simulation of the loading conditions of large strain ranges.

References

ANAHID, M., SAMAL, M. K. & GHOSH, S. 2011. Dwell fatigue crack nucleation model based on crystal plasticity finite element simulations of polycrystalline titanium alloys. *Journal of the Mechanics and Physics of Solids,* 59**,** 2157-2176.

BASSANI, J. L. & WU, T.-Y. 1991. Latent Hardening in Single Crystals II. Analytical Characterization and Predictions. *Proceedings of the Royal Society of London. Series A: Mathematical and Physical Sciences,* 435**,** 21-41.

BIELER, T. R., EISENLOHR, P., ROTERS, F., KUMAR, D., MASON, D. E., CRIMP, M. A. & RAABE, D. 2009. The role of heterogeneous deformation on damage nucleation at grain boundaries in single phase metals. *International Journal of Plasticity,* 25**,** 1655-1683.

CHABOCHE, J. L. 1991. On some modifications of kinematic hardening to improve the description of ratchetting effects. *International Journal of Plasticity,* 7**,** 661-678.

DIARD, O., LECLERCQ, S., ROUSSELIER, G. & CAILLETAUD, G. 2005. Evaluation of finite element based analysis of 3D multicrystalline aggregates plasticity: Application to crystal plasticity model identification and the study of stress and strain fields near grain boundaries. *International Journal of Plasticity,* 21**,** 691-722.

DUNNE, F. P. E., WILKINSON, A. J. & ALLEN, R. 2007. Experimental and computational studies of low cycle fatigue crack nucleation in a polycrystal. *International Journal of Plasticity,* 23**,** 273-295.

ELLYIN, F. 1997. *Fatigue damage, crack growth and life prediction* Chapman & Hall.

HARDER, J. 1999. A crystallographic model for the study of local deformation processes in polycrystals. *International Journal of Plasticity,* 15**,** 605-624.

LE PÉCHEUR, A., CURTIT, F., CLAVEL, M., STEPHAN, J. M., REY, C. & BOMPARD, P. 2012a. Polycrystal modelling of fatigue: Pre-hardening and surface roughness effects on damage initiation for 304L stainless steel. *International Journal of Fatigue,* 45**,** 48-60.

LE PÉCHEUR, A., CURTIT, F., CLAVEL, M., STEPHAN, J. M., REY, C. & BOMPARD, P. 2012b. Thermo-mechanical FE model with memory effect for 304L austenitic stainless steel presenting microstructure gradient. *International Journal of Fatigue,* 45**,** 106-115.

LIN, B., ZHAO, L. G. & TONG, J. 2011. A crystal plasticity study of cyclic constitutive behaviour, crack-tip deformation and crack-growth path for a polycrystalline nickel-based superalloy. *Engineering Fracture Mechanics,* 78**,** 2174-2192.

ROTERS, F., EISENLOHR, P., HANTCHERLI, L., TJAHJANTO, D. D., BIELER, T. R. & RAABE, D. 2010. Overview of constitutive laws, kinematics, homogenization and multiscale methods in crystal plasticity finite-element modeling: Theory, experiments, applications. *Acta Materialia,* 58**,** 1152-1211.